Ecological Applications, 18(4), 2008, pp. 965–982

AQUATIC METABOLISM AND ECOSYSTEM HEALTH ASSESSMENT USING DISSOLVED O_2 STABLE ISOTOPE DIEL CURVES

Jason J. Venkiteswaran,[1,3] Sherry L. Schiff,[1] and Leonard I. Wassenaar[2]

[1]*Department of Earth and Environmental Sciences, University of Waterloo, 200 University Avenue W, Waterloo, Ontario N2G 3L1 Canada*
[2]*Environment Canada, 11 Innovation Boulevard, Saskatoon, Saskatchewan S7N 3H5 Canada*

Abstract. Dissolved O_2 concentration and $\delta^{18}O$-O_2 diel curves can be combined to assess aquatic photosynthesis, respiration, and metabolic balance, and to disentangle some of the confounding factors associated with interpretation of traditional O_2 concentration curves. A dynamic model is used to illustrate how six key environmental and biological parameters interact to affect diel O_2 saturation and $\delta^{18}O$-O_2 curves, thereby providing a fundamental framework for the use of $\delta^{18}O$-O_2 in ecosystem productivity studies. $\delta^{18}O$-O_2 provides information unavailable from concentration alone because $\delta^{18}O$-O_2 and saturation curves are not symmetrical and can be used to constrain gas exchange and isotopic fractionation by eliminating many common assumptions. Changes in key parameters affect diel O_2 saturation and $\delta^{18}O$-O_2 curves as follows: (1) an increase in primary production and respiration rates increases the diel range of O_2 saturation and $\delta^{18}O$-O_2 and decreases the mean $\delta^{18}O$-O_2 value; (2) a decrease in the primary production to respiration ratio (P:R) decreases the level of O_2 saturation and increases the $\delta^{18}O$-O_2 values; (3) an increase in the gas exchange rate decreases the diel range of O_2 saturation and $\delta^{18}O$-O_2 values and moves the mean O_2 saturation and $\delta^{18}O$-O_2 values toward atmospheric equilibrium; (4) a decrease in strength of the respiratory isotopic fractionation (α_R closer to 1) has no effect on O_2 saturation and decreases the $\delta^{18}O$-O_2 values; (5) an increase in the $\delta^{18}O$ of water has no effect on O_2 saturation and increases the minimum (daytime) $\delta^{18}O$-O_2 value; and (6) an increase in temperature reduces O_2 solubility and thus increases the diel range of O_2 saturation and $\delta^{18}O$-O_2 values. Understanding the interplay between these key parameters makes it easier to decipher the controls on O_2 and $\delta^{18}O$-O_2, compare aquatic ecosystems, and make quantitative estimates of ecosystem metabolism. The photosynthesis to respiration to gas exchange ratio (P:R:G) is better than the P:R ratio at describing and assessing the vulnerability of aquatic ecosystems under various environmental stressors by providing better constrained estimates of ecosystem metabolism and gas exchange.

Key words: dissolved oxygen; gas exchange; metabolism; primary production; respiration; stable isotopes.

Introduction

Primary productivity (P) and species richness are commonly used as measures of aquatic ecosystem function. P is the rate of O_2 evolution generated by the photochemical oxidation of water and is associated with the fixation of carbon and energy into plant biomass (Falkowski and Raven 1997). Studies have suggested that dissolved O_2 evolution is a more direct means of estimating P in aquatic systems than conventional carbon-based approaches, since carbon- and O_2-based rates can differ significantly if photorespiratory rates are high or if photosynthetically derived electrons are used to reduce nitrate (Falkowski and Raven 1997). In aquatic systems, the O_2 evolved from P is added to a pre-existing dissolved O_2 pool that is linked to the atmosphere via air–water gas exchange (G). Aquatic community (plant, animal, microbe) respiration (R) processes also occur in that same environment, consume dissolved O_2 from the water column, and generally produce carbon dioxide (CO_2). Employing O_2 evolution to quantify the aquatic P component of ecosystem function requires disentangling the concomitant processes of P, R, and G that ultimately govern the concentration of dissolved O_2 in aquatic ecosystems. Thus, dissolved O_2 evolution and consumption are inherently linked to carbon-flow and food web structure in freshwater and marine ecosystems (Carignan et al. 2000).

Minimum dissolved O_2 concentrations are required for the survival of many aquatic organisms (Chapman 1986, Barton and Taylor 1996). Thus dissolved O_2 is also a primary indicator of aquatic ecosystem health. Whereas dissolved O_2 concentrations in rivers and lakes naturally seek to attain local equilibrium saturation with atmospheric O_2, the overall metabolic balance between

Manuscript received 21 March 2007; revised 29 October 2007; accepted 11 December 2007. Corresponding Editor: B. A. Hungate.

[3] E-mail: jjvenkit@uwaterloo.ca

P and *R* (commonly expressed as a *P*:*R* ratio) can be tilted in either direction (O_2 super- or under-saturation) on a daily to seasonal basis (Odum 1956, del Giorgio and Peters 1994, Rizzo et al. 1996, Carignan et al. 2000). Undersaturated and low dissolved O_2 in wetlands, rivers, streams, lakes, and estuaries result from normal biogeochemical processes (e.g., community *R*), but can be exacerbated by atmospheric reaeration constraints such as extended ice cover. Human activities, such as industrial or nutrient discharges, have detrimental impacts on dissolved O_2 concentrations by increasing biological and chemical O_2 demand or by stimulating algal growth (Wetzel 2001). One adverse outcome of nutrient-driven eutrophication may be temporal anoxia that can result in fish kills or harmful changes in overall community structure either at night, in deeper waters during prolonged thermal stratification, or under sustained ice covered conditions (Carpenter et al. 1998, Dodds and Welch 2000, Welch and Jacoby 2004).

Conventionally, *P* and *R* rates in water bodies are determined during the summer growing season using light and dark bottle incubations, by diel dissolved O_2 concentration curve analysis, and by ^{14}C-CO_2 incubations or ^{18}O-H_2O spike incubations (cf. Falkowski and Raven 1997). Point measurements of O_2 (or CO_2) are ineffective in productive systems because of diel changes in O_2 (and CO_2) concentrations. The analysis of diel dissolved O_2 concentration curves has long been used to estimate *P* and *R* in aquatic systems (Odum 1956, Chapra and Di Toro 1991, Wilcock et al. 1998, Wetzel 2001). More recently, the application of natural abundance stable oxygen isotopic ratios (^{18}O:^{16}O ratio, hereafter in δ-notation relative to standard mean ocean water [SMOW]) in diel studies of aquatic ecosystems has shown that it is possible to separate some of the confounding factors associated with conventional interpretations of diel concentration curves (Parker et al. 2005, Tobias et al. 2007, Venkiteswaran et al. 2007). While ^{17}O analysis has been proven useful in quantifying gross O_2 production integrated over multi-week timescales and in low productivity or high *G* environments (e.g., Luz and Barkan 2000, Hendricks et al. 2005, Sarma et al. 2006), this technique has not been applied to ecosystems with diel cycles.

Coupling the analysis of dissolved O_2 concentration and $\delta^{18}O$-O_2 diel curves is particularly useful in studies of aquatic ecosystem function because the shape, size, and location of dissolved O_2 vs. $\delta^{18}O$-O_2 diel curves provide quantitative information about *P*, *R*, and *G*. A non-steady-state model (PoRGy) was recently developed to quantify dissolved O_2 and $\delta^{18}O$-O_2 evolution in aquatic systems (Venkiteswaran et al. 2007). *P*, *R*, *G*, and other key measured environmental parameters were used to generate and fit diel curves to field dissolved O_2 and $\delta^{18}O$-O_2 data in a variety of aquatic ecosystems. The PoRGy model allows researchers to construct and test O_2-based hypotheses to decipher aquatic metabolism, metabolic balance, and reaeration under dynamic conditions. Since the natural abundance O_2 isotope approach to aquatic metabolism studies is still relatively new, the objective of this paper is to examine in detail the effects of the key environmental parameters on the shape, size, and magnitude of diel curves of dissolved O_2 and $\delta^{18}O$-O_2 curves, which are intrinsic indicators of ecosystem health. Five generalized *P*:*R* stream clusters that cover a majority of the aquatic ecosystem health scenarios likely to be encountered in nature are used to illustrate these effects. These stream clusters were then compared with diel field data from several North American aquatic ecosystems. Importantly, researchers are provided with a fundamental framework to guide the use of dissolved O_2 and $\delta^{18}O$-O_2 patterns in ecosystem productivity studies of both natural and altered water bodies.

Methods

$\delta^{18}O$-O_2 fundamentals

Photosynthesis adds dissolved O_2 to aquatic systems. The processes of oxidizing H_2O molecules to produce O_2 does not fractionate between the oxygen isotopes ($\alpha_P = 1.000$ [Stevens et al. 1975, Guy et al. 1989, 1993], where α is the isotope fractionation factor defined as the ^{18}O:^{16}O ratio of the product to that of the reactant). As a result, *P* generally decreases the ambient $\delta^{18}O$-O_2 value by adding O_2 with the same $\delta^{18}O$ value as the H_2O. The $\delta^{18}O$-O_2 decreases because the $\delta^{18}O$-H_2O is typically much lower than atmospheric $\delta^{18}O$-O_2. *P* is controlled by the combination of photosynthetically active radiation (PAR), temperature, abundance of photosynthetic organisms, and other factors (Wetzel 2001).

Conversely, *R* decreases the dissolved O_2 concentration and increases the $\delta^{18}O$-O_2 value because of the preferential consumption (fractionation) of the light O_2 isotopologue ($^{16}O^{16}O$), and is controlled by many factors including carbon and nutrient availability, temperature, and the abundance of respiring organisms (Lane and Dole 1956, Wetzel 2001). In practice, ecosystem measurements of *R* include all O_2 consuming pathways such as microbial *R*, photorespiration, the Mehler-peroxidase reaction, chlororespiration, and chemical and photochemical O_2 demand. All of these pathways preferentially consume the light O_2 isotopologue (cf. Miles and Brezonik 1981, Andrews et al. 2000, Laws et al. 2000, Bennoun 2002, Venkiteswaran et al. 2007, Chomicki and Schiff 2008). The magnitude of the dissolved O_2 community *R* isotopic fractionation factor (α_R) is a function of the type of aquatic respiring community and the factors that affect *R* rates.

While *P* and *R* are key expressions of aquatic community structure, *G* is a physical process that independently drives O_2 and $\delta^{18}O$-O_2 values from under- or supersaturated conditions toward temperature-dependent air–water equilibrium saturation. *G* is controlled by gas exchange coefficients (*k*) for each O_2 isotopologue based on the thin boundary layer equation $G = k \times (O_{2sat} - O_2)$ where the difference between O_2

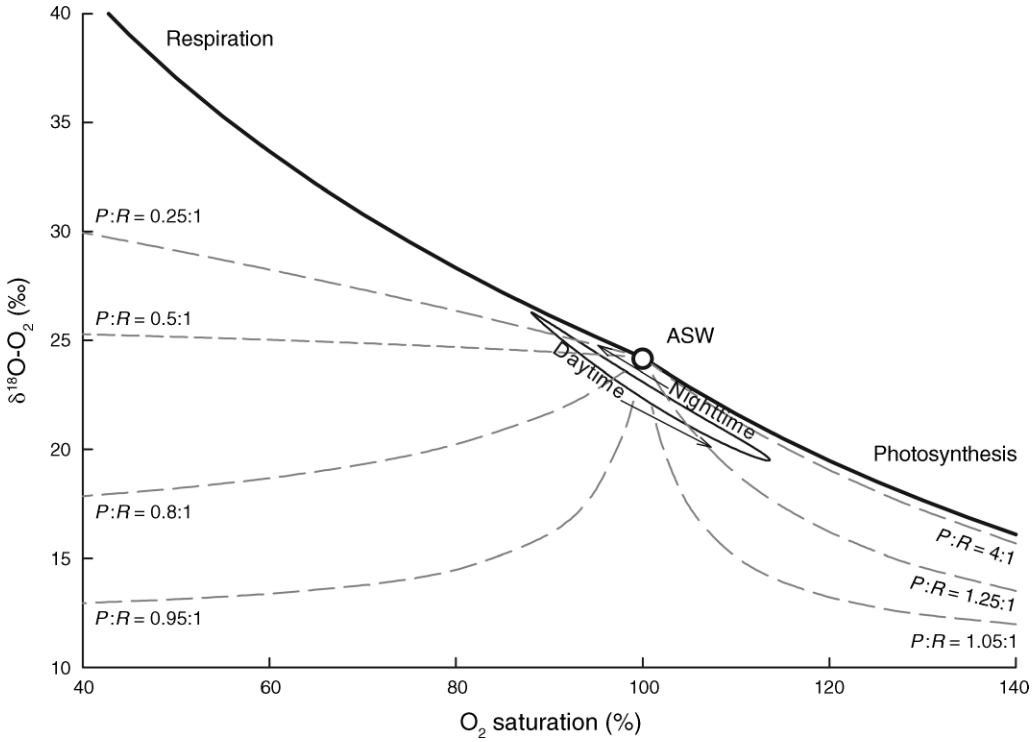

FIG. 1. A graphical depiction of the primary O_2 processes vs. the $\delta^{18}O$-O_2 (deviation from standard mean oceanic water [SMOW]) showing several P:R ratio lines (dashed gray lines) calculated with the steady-state model of Quay et al. (1993) and dissolved O_2 community R isotopic fractionation factor $\alpha_R = 0.982$ and $\delta^{18}O$-$H_2O = -7‰$. The respiration and photosynthesis end-member trajectories (solid black lines) were also calculated with $\alpha_R = 0.982$ and $\delta^{18}O$-$H_2O = -7‰$ and are shown as moving away from air-saturated water (ASW). The closed loop is a PoRGy model-generated diel curve with P, R, and G of 288, 300, and 178 $mg \cdot m^{-2} \cdot h^{-1}$ (P:R:G = 1.61:1.68:1) and k of 0.24 m/h, which yields a range of about 25% in saturation and 6‰ in $\delta^{18}O$-O_2. P is the rate of photosynthetic O_2 evolution generated by the photochemical oxidation of water; R is aquatic community (plant, animal, microbe) respiration, G is air–water gas exchange, k is the gas exchange coefficient, and PoRGy is a non-steady-state model that was developed to quantify dissolved O_2 and $\delta^{18}O$-O_2 evolution in aquatic systems (Venkiteswaran et al. 2007).

saturation and the actual O_2 concentrations is multiplied by k. There is a small equilibrium isotope fractionation between the $\delta^{18}O$-O_2 of the atmosphere and the $\delta^{18}O$-O_2 of dissolved O_2 whereby the latter is about 0.7‰ greater than the former ($\alpha_{G\text{-eq}} = 1.0007$ [Benson et al. 1979]). Since the $\delta^{18}O$-O_2 value of atmospheric O_2 is globally constant at +23.5‰ (Kroopnick and Craig 1972), dissolved O_2 in saturation equilibrium with the atmosphere and in the absence of P and R will have a $\delta^{18}O$-O_2 value of about +24.2‰. The measured kinetic isotopic fractionation factor for O_2 invasion–evasion ($\alpha_{G\text{-}k} = 0.9972$ [Knox et al. 1992]) means that k for the heavy O_2 isotopologue ($^{18}O^{16}O$) is about 3‰ slower than for the light O_2 isotopologue ($^{16}O^{16}O$).

Plots of dissolved O_2 saturation vs. $\delta^{18}O$-O_2 are particularly useful for comparing aquatic systems with different P, R, and G because the data are normalized for temperature. The shape, size, and location of a diel curve in a cross-plot of O_2 saturation vs. $\delta^{18}O$-O_2 arises from the combined effects of different P, R, and G, and their respective O_2 isotopic fractionation factors that are ecosystem specific (Fig. 1). Steady-state models have used these cross-plots to display data and estimate P:R (e.g., Quay et al. 1993). However, transient steady state P:R lines are not linear and the space between them varies as a function of O_2 saturation, $\delta^{18}O$-O_2, and P:R itself. Thus estimating the P:R of an ecosystem or comparing ecosystems without understanding the effects of individual parameters would be very difficult. Three key features of these cross-plots are that P:R lines are curvilinear and not readily apparent from only the O_2 saturation and $\delta^{18}O$-O_2 axes, diel curves cross many P:R lines, and the daytime and nighttime portions of the curve are not identical. The effects of six key metabolic and environmental parameters on the shape, size, location, and mean of diel curves are examined: (1) different P and R but the same P:R; (2) widely differing P:R; (3) different gas exchange coefficients, k; (4) different community respiration isotopic fractionation factors, α_R; (5) different $\delta^{18}O$-H_2O values; and (6) different water temperature regimes.

Diel curves

Diel changes in dissolved O_2 concentration in well-mixed surface water bodies are not sinusoidal. Following sunrise, dissolved O_2 concentrations increase due to

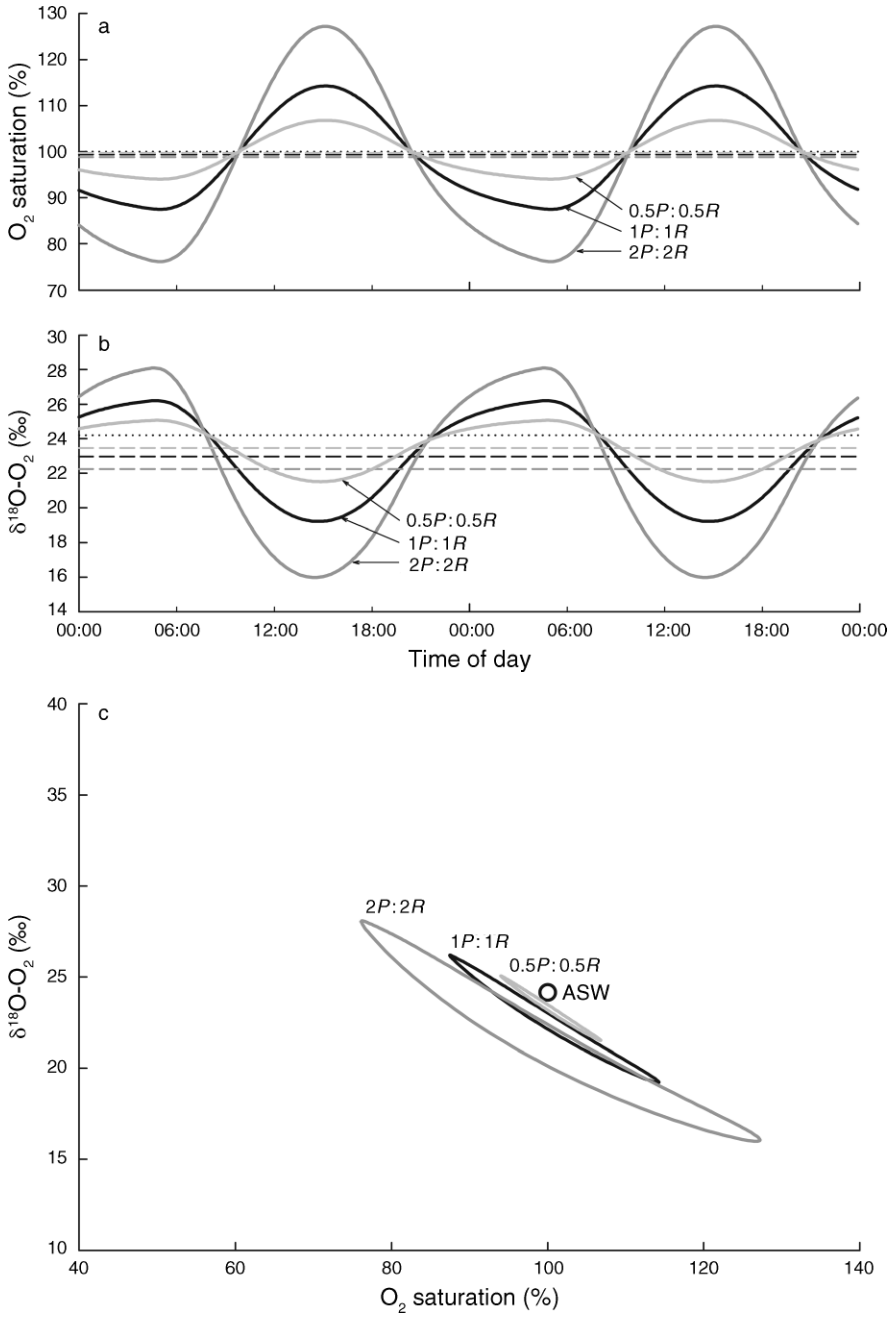

FIG. 2. Diel curves show how different rates of P and R affect the shape, size, and location of the O_2 and $\delta^{18}O$-O_2 curves when the P:R ratio is held constant. Three diel curves with the same gas exchange rate and identical P:R ratios, but with different P and R are shown. The solid curve from Fig. 1 (1P:1R, 288:300 mg·m^{-2}·h^{-1}, black) is compared to curves with half those rates (0.5P:0.5R, 144:150 mg·m^{-2}·h^{-1}, dark gray) and with double those rates (2P:2R, 576:600 mg·m^{-2}·h^{-1}, light gray). In (a) and (b), the mean of each diel curve is shown as a dashed line; air-saturated water (ASW) is shown as a dotted line. In (c), ASW is shown as a black circle.

photosynthetic inputs and can approach a quasi-steady state plateau where P, R, and G are balanced. However, in reality very few productive aquatic systems reach steady-state conditions during the daytime because of changing PAR and other dynamic factors such as water temperature. As illumination declines and R exceeds P, dissolved O_2 concentrations decline and can approach a steady-state concentration during the nighttime when R is offset by an equal O_2 influx by G (re-aeration). As a result of the dynamic changes in P and R, diel dissolved O_2 concentration curves tend to be saw-toothed, rather than sinusoidal (Venkiteswaran et al. 2007).

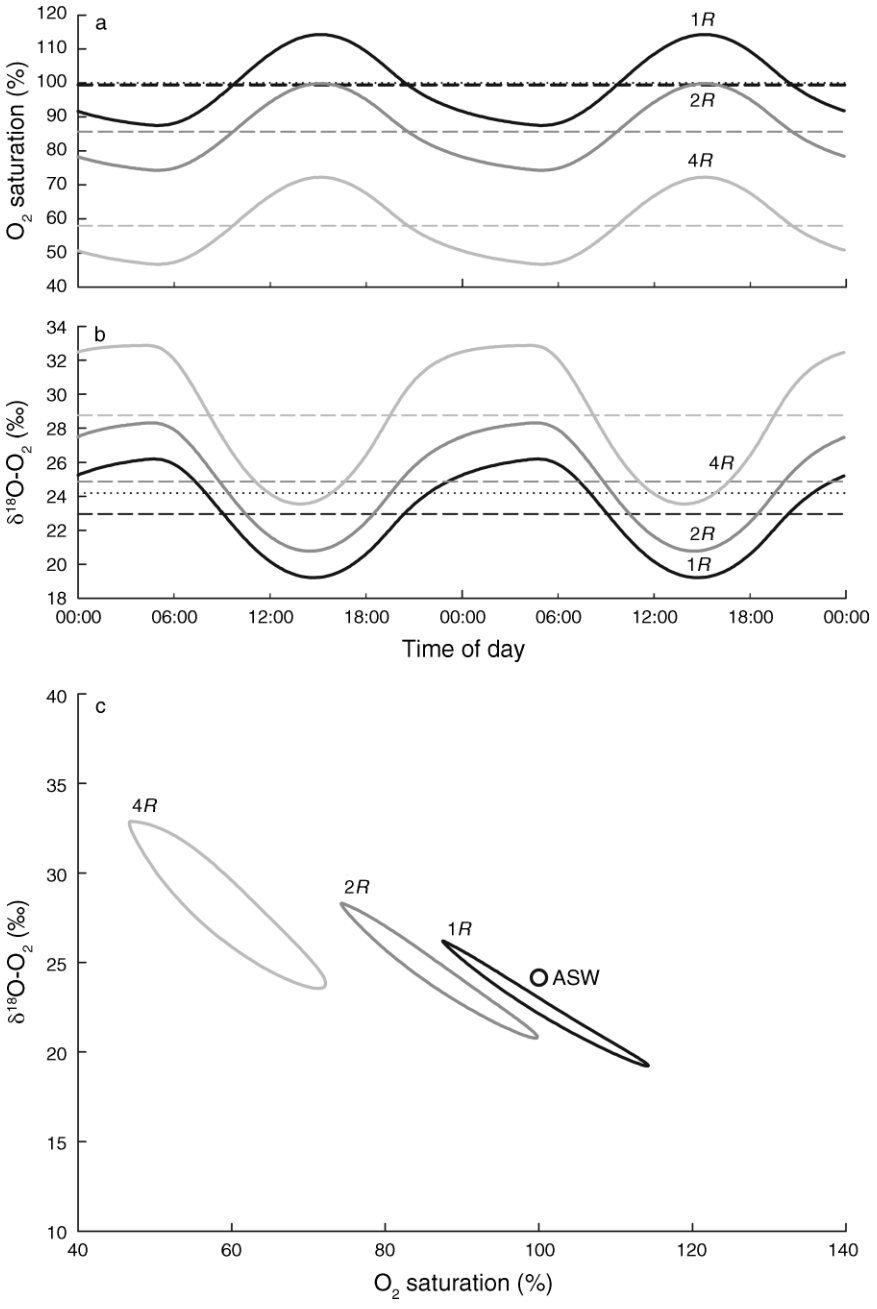

FIG. 3. Diel curves show how different rates of R affect the shape, size, and location of the O_2 and $\delta^{18}O$-O_2 curves when the P:R ratio is increased and P and k are held constant. The solid curve from Fig. 1 ($1R$, 300 mg·m^{-2}·h^{-1}, black) is compared to curves with double that respiration rate ($2R$, 600 mg·m^{-2}·h^{-1}, dark gray) and quadruple that respiration rate ($4R$, 1200 mg·m^{-2}·h^{-1}, light gray). In (a) and (b), the mean of each diel curve is shown as a dashed line; air-saturated water (ASW) is shown as a dotted line. In (c), ASW is shown as a black circle.

Diel curves of dissolved O_2 and $\delta^{18}O$-O_2 are rarely exact mirror images of each other. Following sunrise, the addition of O_2 with very low $\delta^{18}O$-O_2 values from P decreases the dissolved $\delta^{18}O$-O_2 value in the water column. The $\delta^{18}O$-O_2 minimum cannot occur before the O_2 concentration maximum unless there is a large water temperature decrease during the day. Following solar noon, P decreases and R causes an increase in the dissolved $\delta^{18}O$-O_2. The $\delta^{18}O$-O_2 value can approach a steady-state value during nighttime that is related not only to the R:G ratio, but is also controlled by α_R. As a result, differences in the diel shape between dissolved O_2 and $\delta^{18}O$-O_2, in addition to the temporal offset between dissolved O_2 and $\delta^{18}O$-O_2 curves, give crucial information that can be exploited to quantify P, R, G, and α_R in aquatic ecosystems.

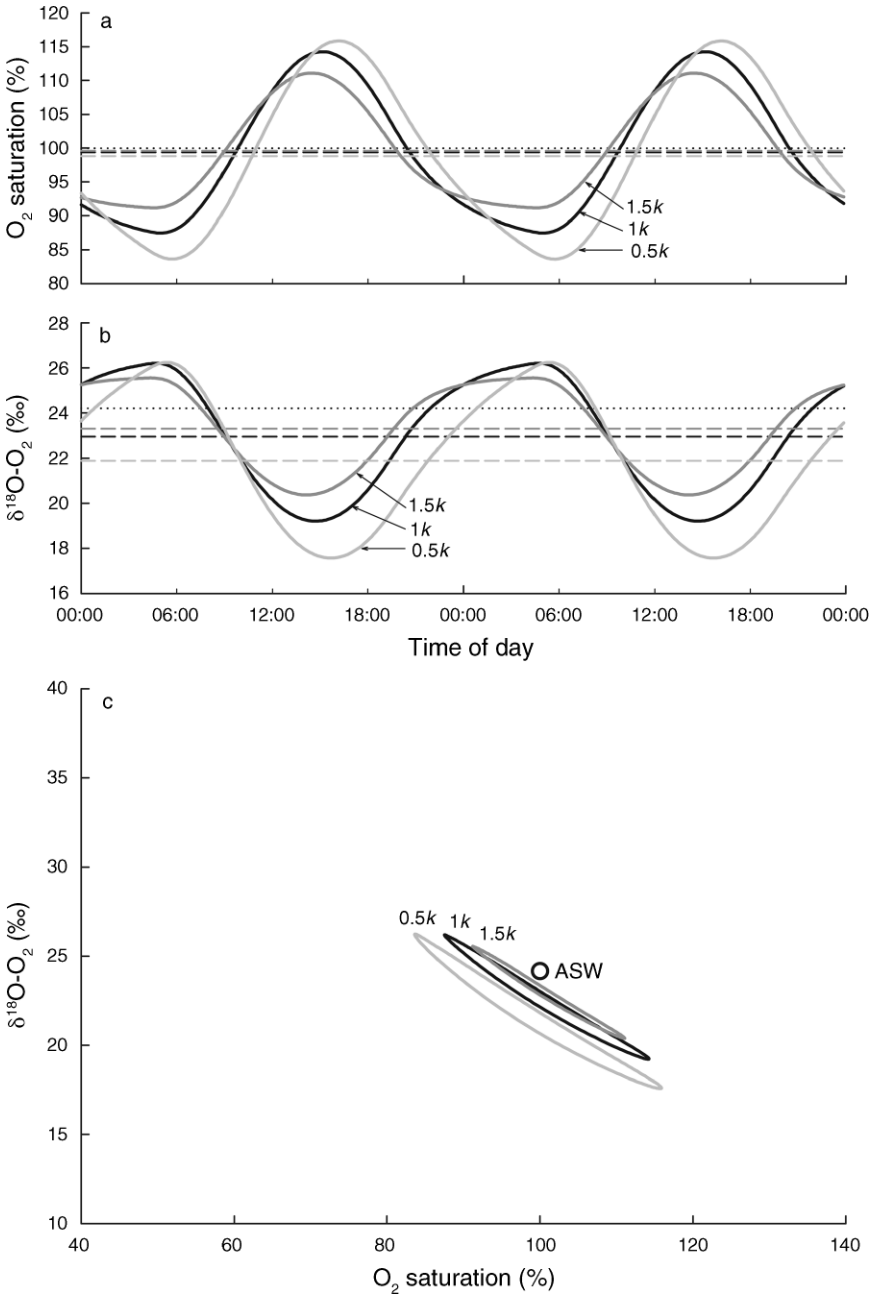

FIG. 4. Diel curves show how different gas exchange coefficients (k) affect the shape, size, and location of the curves when the P:R ratio and P and R are held constant. The solid curve from Fig. 1 (1k, 0.24 m/h, black) is compared to curves with increased k (1.5k, 0.36 m/h, dark gray) and decreased k (0.5k, 0.12 m/h, light gray). In (a) and (b), the mean of each diel curve is shown as a dashed line; air-saturated water (ASW) is shown as a dotted line. In (c), ASW is shown as a black circle.

The environmental conditions and depictions in this manuscript are diel steady-state model solutions using the above parameters and PoRGy (Venkiteswaran et al. 2007). The daytime and nighttime portions of the diel curve follow different trajectories and cross many of the non-diel steady-state P:R lines. Representative values of P, R, and k for the model aquatic ecosystem (Fig. 1) were chosen to (1) provide a sufficiently large range of O_2 saturation and $\delta^{18}O$-O_2 to demonstrate the effects; (2) portray a moderate level of metabolic activity typical of natural systems; and (3) represent a moderate gas exchange rate. If P and R are changed, G is also changed even when k is held constant because G depends on O_2 saturation and k. Thus all comparisons of G are presented in terms of k.

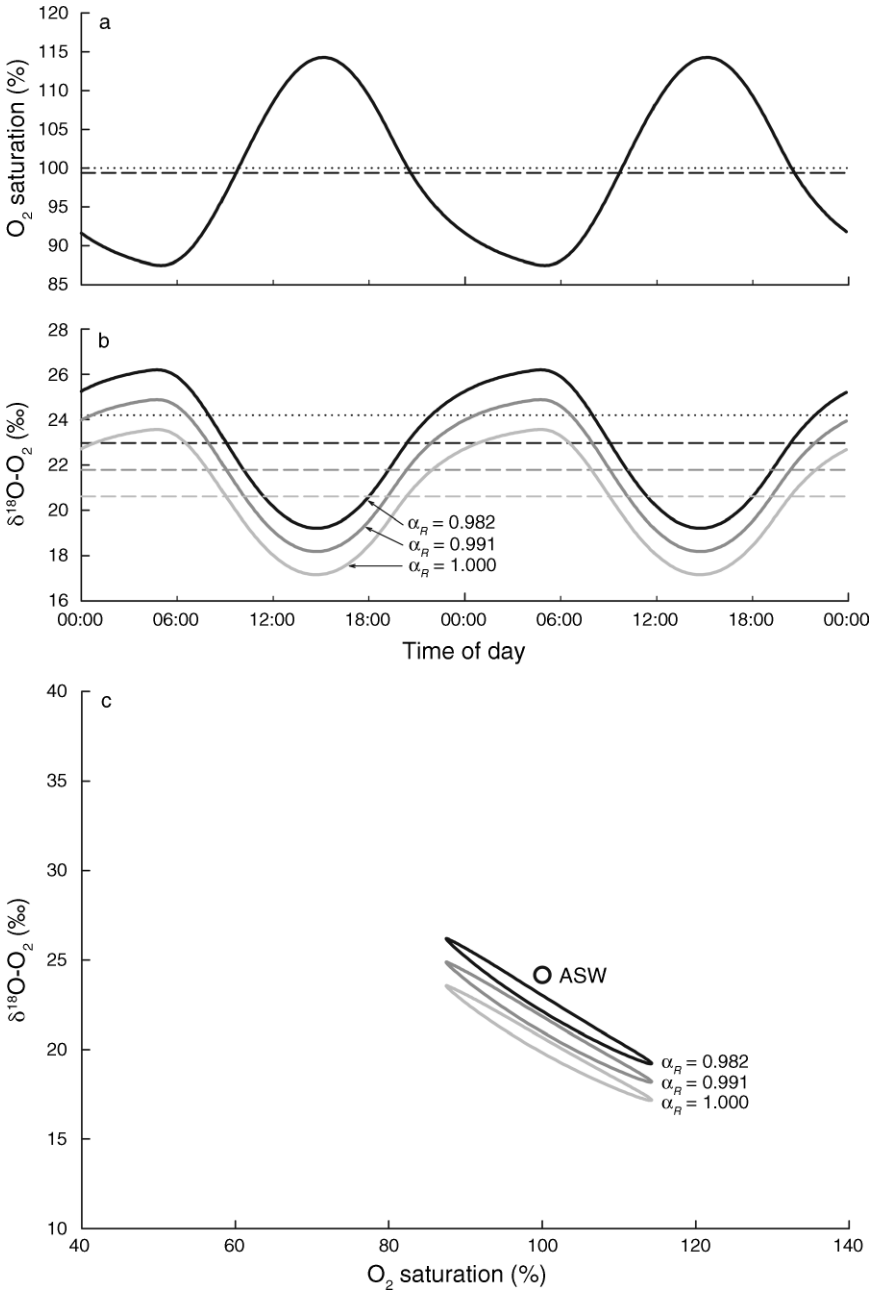

FIG. 5. Diel curves show how O_2 isotopic fractionation factors (α_R) affect the shape, size, and location of the curves when the *P*:*R* ratio, *P*, *R*, and *k* are held constant. The solid curve Fig. 1 ($\alpha_R = 0.982$, black) is compared to curves with $\alpha_R = 0.988$ (dark gray) and $\alpha_R = 0.995$ (light gray). In (a) and (b), the mean of each diel curve is shown as a dashed line; air-saturated water (ASW) is shown as a dotted line. In (c), ASW is shown as a black circle.

RESULTS

Effect of metabolic rates on diel O_2 and $\delta^{18}O$-O_2

Community metabolic rates control the deviation of diel $\delta^{18}O$-O_2 curves from air–water equilibrium saturation. Increasing *P* and *R*, while retaining a constant *P*:*R* (Fig. 2a, b), produces diel curves of O_2 saturation and $\delta^{18}O$-O_2 with a larger amplitude that progressively deviate farther from equilibrium saturation. This finding clearly demonstrates that the widespread and historical practice of reporting *P*:*R* alone reveals very little about the true productivity of an aquatic ecosystem. In O_2 saturation vs. $\delta^{18}O$-O_2 space (Fig. 2c), increases in *P* and *R* result in (1) an increase the length of the diel curve; (2) an increase in the difference between the daytime and nighttime portions of the curve; and (3) placement of the curve farther away from air–water equilibrium saturation. Higher rates of community

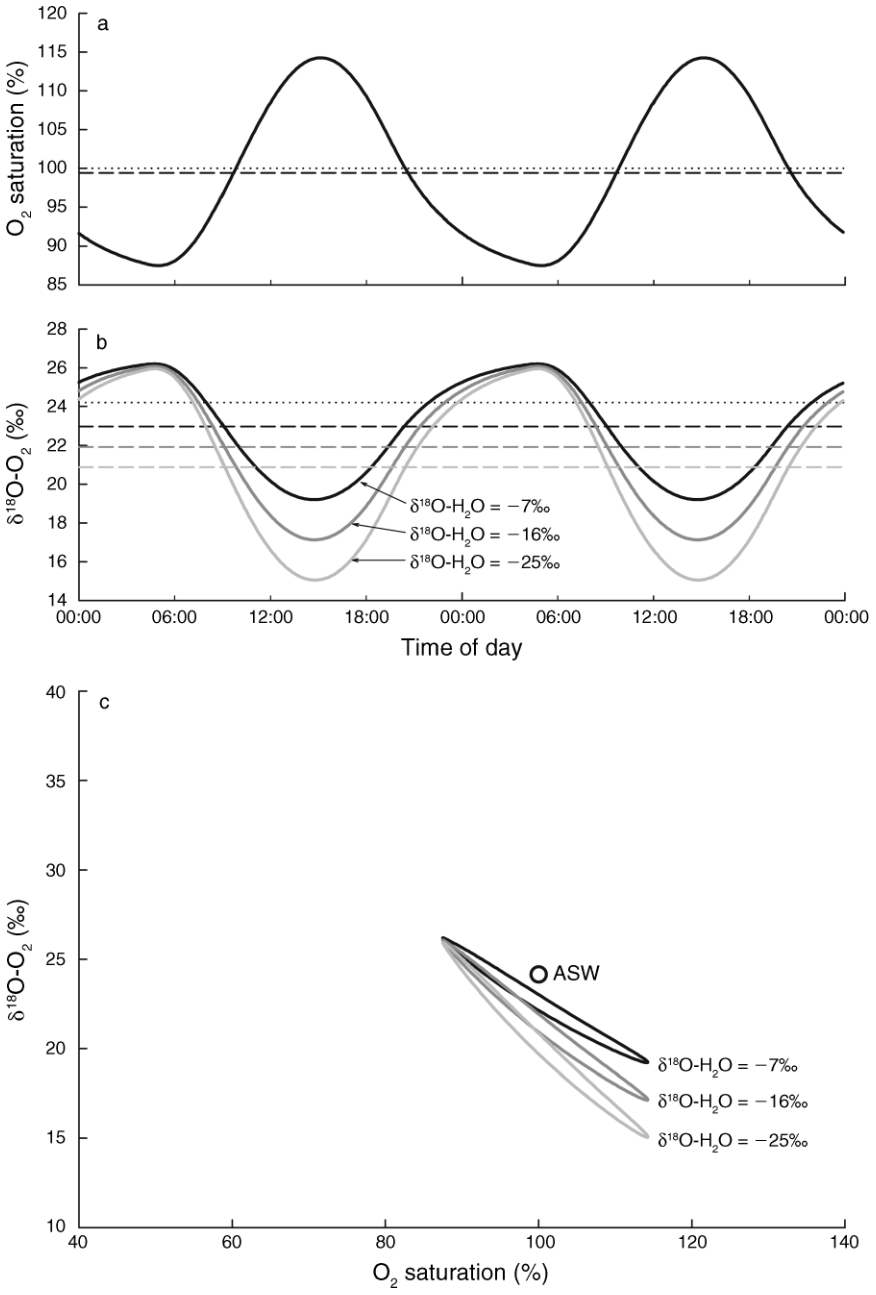

FIG. 6. Diel curves show how different $\delta^{18}O$-H_2O values affect the shape, size, and location of the curves when the *P*:*R* ratio, *P*, *R*, and *k* are held constant. The solid curve from Fig. 1 ($\delta^{18}O$-$H_2O = -7‰$, black) is compared to curves with $\delta^{18}O$-$H_2O = -14‰$ (dark gray) and $\delta^{18}O$-$H_2O = -21‰$ curve (light gray). In (a) and (b), the mean of each diel curve is shown as a dashed line; air-saturated water (ASW) is shown as a dotted line. In (c), ASW is shown as a black circle.

metabolism have little effect on the daily mean O_2 saturation, but significantly reduce the daily mean $\delta^{18}O$-O_2 value.

Effect of community respiration rate on diel O_2 and $\delta^{18}O$-O_2

To illustrate the effect of increasing *R*, *P* and *k* were held constant and thus *P*:*R* decreased. In water bodies, *R* may increase relative to *P* as a result of warming water temperatures over the course of the day or season, input of allochthonous labile organic carbon from streams or tile drains, and from the seasonal changes in phytoplankton that deliver organic carbon to respiring organisms. *R* controls several aspects of the shape and location of the diel curve in O_2 saturation vs. $\delta^{18}O$-O_2 space (Fig. 3c). The main effect of increasing *R* relative to *P* is to (1) decrease the daily mean O_2 saturation level without changing the shape and amplitude of the diel

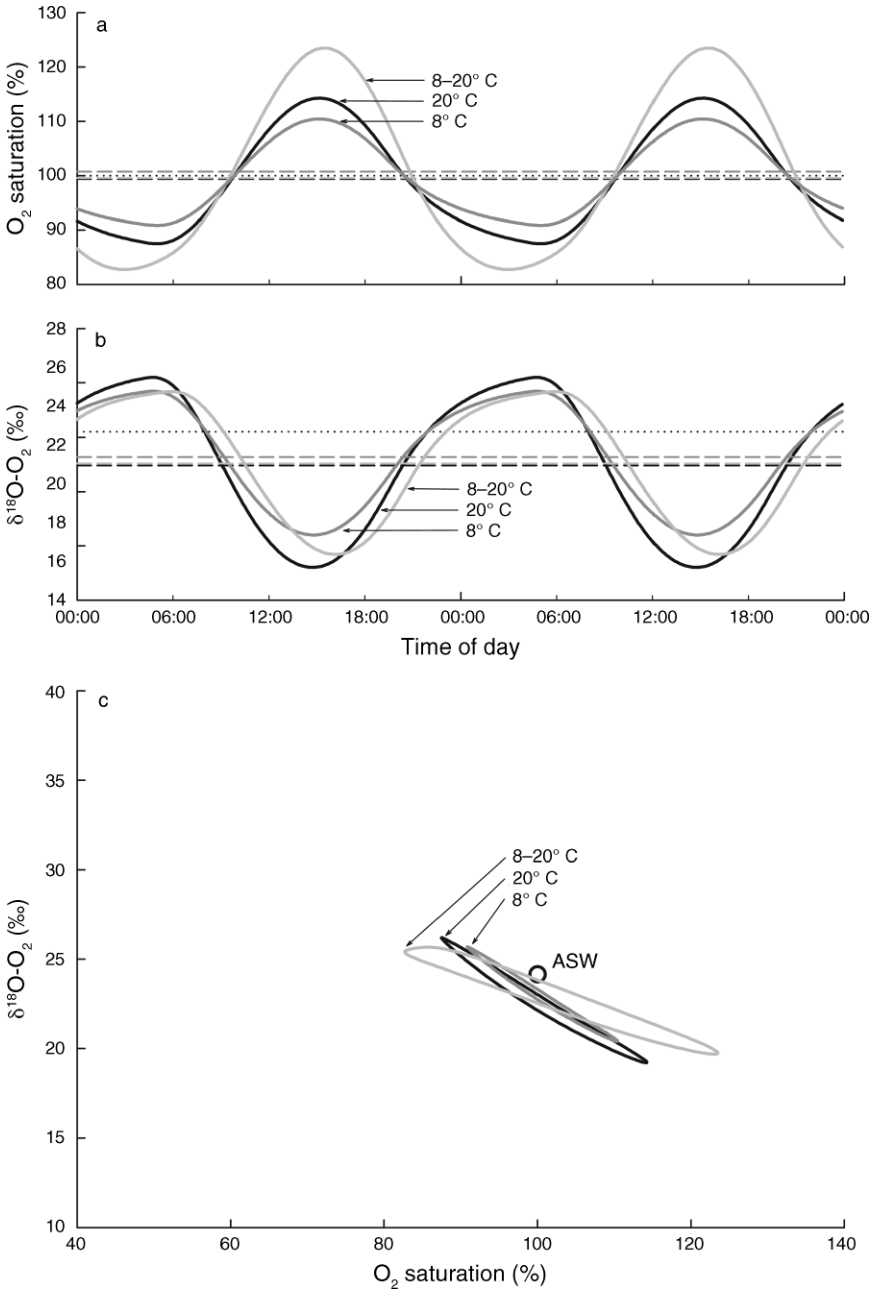

FIG. 7. Diel curves show how different temperatures affect the shape, size, and location of the curves when the *P*:*R* ratio, *P*, *R*, and *k* are held constant. The solid curve from Fig. 1 (20°C, black) is compared to curves with a colder water temperature (8°C, dark gray) and a diel water temperature change (8° to 20°C, light gray). In (a) and (b), the mean of each diel curve is shown as a dashed line; air-saturated water (ASW) is shown as a dotted line. In (c), ASW is shown as a black circle.

curve; (2) increase the daily mean $\delta^{18}O$-O_2 value and to increase the diel range of $\delta^{18}O$-O_2 values; and (3) enhance the nighttime $\delta^{18}O$-O_2 plateau. The nighttime plateau is much more pronounced than a daytime plateau because of the different effects of $\delta^{18}O$-H_2O and α_R.

The development of a nighttime plateau is a very important feature of diel $\delta^{18}O$-O_2 data because it provides clues about the aquatic ecosystem before any modeling is done. A nighttime plateau in O_2 saturation is the result of *R* and *G* being equal. The $\delta^{18}O$-O_2 value of a nighttime plateau is a function of *R* and α_R. Such a nighttime plateau in $\delta^{18}O$-O_2 only occurs when *R* is sufficiently large and of similar magnitude as *G*.

Higher aquatic *R* affects the O_2 saturation and $\delta^{18}O$-O_2 curves differently. An increase in *R* affects the amplitude

TABLE 1. Summary of the effect the six key parameters on O_2 saturation and $\delta^{18}O$-O_2 values.

Change in variable	O_2 saturation			$\delta^{18}O$-O_2		
	Maximum	Minimum	Mean	Maximum	Minimum	Mean
Increase metabolism (P and R)	increase	decrease	no change	increase	decrease	decrease
Increase P	increase	decrease	increase	no change	decrease	decrease
Increase R	decrease	decrease	decrease	increase	increase	increase
Increase G (as k)	decrease	increase	increase (slightly)	decrease	increase	increase
Increase α_R (closer to 1)	no change	no change	no change	decrease	decrease	decrease
Increase T	increase	decrease	decrease	increase	decrease	decrease
Increase $\delta^{18}O$-H_2O	no change	no change	no change	no change	increase	increase

Note: P is the rate of photosynthetic O_2 evolution generated by the photochemical oxidation of water; R is aquatic community (plant, animal, microbe) respiration, G is air–water gas exchange, k is the gas exchange coefficient, and T is temperature.

of the diel $\delta^{18}O$-O_2 curve, but not the amplitude of the diel O_2 saturation curve. Thus the range of the $\delta^{18}O$-O_2 is an indicator of P:R. In O_2 saturation vs. $\delta^{18}O$-O_2 space (Fig. 3c), the effect of increasing R is to (1) move the diel curve to the left and upward; and (2) increase the difference between the daytime and nighttime portions of the diel curve.

Effect of gas exchange coefficient on diel O_2 and $\delta^{18}O$-O_2

The gas exchange coefficient, k, controls several aspects of the shape of the diel O_2 saturation and $\delta^{18}O$-O_2 curves (Fig. 4). The k values used here (0.12–0.36 m/h) cover a reasonable range of moderate-k environments such as larger lakes and rivers and higher-k environments such as turbulent streams and rivers (e.g., a large windy lake [12 m/s wind speed at 10 m height; Wanninkhof 1992] and moderately moving streams [1 m/s mean velocity and 1 m depth; Churchill et al. 1962]). In some aquatic ecosystems, k can be estimated via proxy measurements such as wind speed for lakes (e.g., Wanninkhof 1992, Cole and Caraco 1998) or directly by gas tracer and acoustic methods (Morse et al. 2007). In streams and rivers, numerous empirical equations can be used to estimate k for different hydrologic settings based on easily measured variables, such as channel depth and mean water velocity (e.g., Jha et al. 2004). However, literature k values can vary by up to several orders of magnitude for any given circumstance (e.g., O'Connor and Dobbins 1958, Churchill et al. 1962, Jha et al. 2004).

G acts primarily to dampen the magnitude of the diel O_2 saturation and $\delta^{18}O$-O_2 swings driven by P and R. In general, the proximity of the diel curve to equilibrium saturation conditions is controlled by k, and thus G. The amount of hysteresis exhibited by the diel curves is partially controlled by the P:G ratio, such that if P:G is small, then the difference between the daytime and nighttime portion of the diel curves is small and the total range of O_2 saturation and $\delta^{18}O$-O_2 values is also small. Thus, the net effect of increasing the k value is to (1) increase G, (2) move the diel curve closer to air–water equilibrium saturation, (3) decrease the magnitude of the diel curve, (4) change the shape of the diel curve and especially the appearance of a nighttime plateau, and (5) affect the timing of both O_2 saturation and $\delta^{18}O$-O_2 minima and maxima. The temporal offset between solar

TABLE 2. Stream clusters as described by Wilcock et al. (1998).

Cluster	Ecological description (Wilcock et al. 1998)	P ($g \cdot m^{-3} \cdot d^{-1}$)	R ($g \cdot m^{-3} \cdot d^{-1}$)
1	warmer than average; large diel changes in O_2 concentration; high risk of low O_2 concentrations; small changes in flow can effect low O_2 concentrations at night (due to reduced k and increased R); sensitive to temperature change, and nutrient and organic loading ($n = 7$ streams)	$P \gg R$ (24.8)	below average (9.9)
2	low risk for low O_2 concentrations; susceptible to changes in riparian management coupled with low k during droughts ($n = 7$ streams)	low P (7.3)	low R (8.4)
3	warmer than average; large diel changes in O_2 concentration; moderate risk of low O_2 concentrations tempered by high k ($n = 6$ streams)	high P (38.9)	high R (38.1)
4	cooler than average; less productive than average; shady riparian area; low risk of low O_2 concentrations ($n = 6$ streams)	$P \leq R$ (11.2)	$\geq$average (24.5)
5	high k value keeps streams well oxygenated; low risk of low O_2 concentrations ($n = 2$ streams)	high P (63.3)	high R (47.5)

Notes: See Fig. 8 for diel O_2 saturation and $\delta^{18}O$-O_2 curves of each cluster. P is the rate of photosynthetic O_2 evolution generated by the photochemical oxidation of water; R is aquatic community (plant, animal, microbe) respiration, G is air–water gas exchange, k is the gas exchange coefficient. PoRGy is a non-steady-state model that was developed to quantify dissolved O_2 and $\delta^{18}O$-O_2 evolution in aquatic systems (Venkiteswaran et al. 2007).

† Values of k were converted from units of d^{-1} to m/h (for use in PoRGy) by multiplying by average stream cluster depth.

TABLE 1. Extended.

O_2 saturation (x-axis in the cross-plot)	$\delta^{18}O$-O_2 (y-axis in the cross-plot)	Change in cross-plot shape
increases range	increases range and decreases mean	lengthen and broaden
moves curve to the right	moves curve down	tilt and lengthen
moves curve to the left	moves curve up	broaden and tilt
decreases range and moves curve toward 100%	decreases range and moves curve toward +24.2‰	shorten and narrow
no effect	moves curve up	very small tilt
moves left and increases range	increases range	lengthen and broaden
no effect	increases minimum	tilt and lengthen

noon and the O_2 maximum is sometimes used to calculate k from O_2 curve analysis (McBride and Chapra 2005). Higher k brings the daily mean O_2 saturation and $\delta^{18}O$-O_2 values closer to air–water equilibrium saturation. However, the daily means do not scale linearly with k because G depends on saturation. In O_2 saturation vs. $\delta^{18}O$-O_2 space (Fig. 4c), the effects of increasing k are to (1) decrease the length of the diel curve and (2) decrease the difference between the daytime and nighttime portions of the curve.

Effect of community respiration isotopic fractionation on diel O_2 and $\delta^{18}O$-O_2

The community R O_2 isotopic fractionation factor (α_R) only affects $\delta^{18}O$-O_2 and not O_2 saturation. Thus α_R controls the placement of the diel curve on the $\delta^{18}O$-O_2 axis and has no effect on O_2 concentration or saturation. Fig. 5a, b depicts three diel curves with α_R values that range from 0.982 to 1.000. This range of α_R spans the range reported in the literature for natural aquatic systems, including those that are O_2 diffusion-limited (cf. Kiddon et al. 1993, Brandes and Devol 1997). As the respiratory isotopic fractionation becomes weaker (α_R approaches 1), the diel ellipse falls lower on the $\delta^{18}O$-O_2 axis. Also, the slope of the diel ellipse decreases slightly as α_R approaches 1.000. In Fig. 5c, the change in slope produces differences in $\delta^{18}O$-O_2 that are within the measurement error of continuous-flow isotope-ratio mass spectrometry. When $\alpha_R = 1.000$, the steady-state diel curve must fall entirely below the air–water equilibrium saturation $\delta^{18}O$ value of +24.2‰. The α_R can approach 1.000 in O_2 diffusion-limited aquatic ecosystems with high R such as those dominated by benthic or sediment respiration (Brandes and Devol 1997, Hendry et al. 2002).

The diel $\delta^{18}O$-O_2 curve is sensitive to small changes in α_R; in Fig. 5, a 0.001 change in α_R shifts the $\delta^{18}O$-O_2 values by about 0.13‰. Although community α_R is unknown for any given aquatic ecosystem, it can be estimated within a reasonable range for water columns and is constrained by best-fit modeling of the nighttime plateau (the plateau $\delta^{18}O$-O_2 value depends on α_R) and by best-fit modeling of 24-h diel data (Venkiteswaran et al. 2007). Alternately, others have used closed-system bottle incubation experiments to estimate α_R for water

TABLE 2. Extended.

G (as k, d^{-1})†	O_2 saturation (x-axis in the cross-plot)	$\delta^{18}O$-O_2 (y-axis in the cross-plot)	P:R:G and P:R (from PoRGy)
below average (1.1)	low saturation at night; large range; always undersaturated	large range; centered around 20‰	P:R:G = 4.9:6.0:1 P:R = 0.81:1
below average (3.8)	small range; always undersaturated	small range; centered around 22‰	P:R:G = 3.0:4.0:1 P:R = 0.74:1
≥average (8.1)	low saturation at night; large range; always undersaturated	large range, centered around 26‰	P:R:G = 0.7:1.7:1 P:R = 0.42:1
≥average (11.0)	small range; always undersaturated	small range; centered around 26‰	P:R:G = 0.5:1.5:1 P:R = 0.33:1
high k (26.5)	large range; supersaturated during the day; undersaturated at night	large range; centered around 23‰	P:R:G = 1.2:1.6:1 P:R = 0.75:1

bodies (e.g., Quay et al. 1995), although those results are biased to water column R.

Effect of $\delta^{18}O$-H_2O on diel O_2 and $\delta^{18}O$-O_2

The O_2 saturation curve is unaffected by the $\delta^{18}O$-H_2O. The $\delta^{18}O$-H_2O instead controls the $\delta^{18}O$-O_2 minimum and therefore the slope of the entire hysteretic diel curve (Fig. 6c). At a river station or within a lake it is unlikely that there are significant differences of more than 1‰ in $\delta^{18}O$-H_2O over the course of a few diel cycles. Barring large precipitation or reservoir discharge events, evaporation over a few days is insufficient to change the $\delta^{18}O$-H_2O of water bodies such as streams, rivers, and lakes (cf. Clark and Fritz 1997). The $\delta^{18}O$-H_2O, however, becomes an important variable when comparing results among different water bodies from different geographic locations. Locally, the $\delta^{18}O$-H_2O value of a water body may be temporally altered by snowmelt runoff, storm events, and evaporation. Fig. 6a, b depicts three diel curves with $\delta^{18}O$-H_2O values ranging from −21‰ to −7‰, representing a range that covers values observed globally in freshwater lakes and rivers (Bowen et al. 2005; data *available online*).[4] The nighttime $\delta^{18}O$-O_2 maximum is unaffected by the $\delta^{18}O$-H_2O value, acts as a fixed pivot-point for diel curves of different $\delta^{18}O$-H_2O values, and is, instead, controlled by α_R:α_G ratios (i.e., both the α_R:$\alpha_{G\text{-}k}$ and α_R:$\alpha_{G\text{-eq}}$ ratios). The more negative the $\delta^{18}O$-H_2O, the more negative the minimum $\delta^{18}O$-O_2 because of the photosynthetic input of $\delta^{18}O$-O_2 derived from H_2O. The $\delta^{18}O$-H_2O from many locations can be easily measured or may be estimated from existing databases (Kendall and Coplen 2001). However, when comparing among different aquatic ecosystems, diel $\delta^{18}O$-O_2 curves will be different if the $\delta^{18}O$-H_2O values are different.

Effect of temperature on diel O_2 and $\delta^{18}O$-O_2

Temperature controls several key aspects of the shape of the diel curve largely because of the role of temperature in the solubility of O_2 and R (Fig. 7). Fig. 7a, b depicts three diel curves with different water temperature regimes that are typical of the open-water season in temperate lakes and rivers. The curves shown include two constant water temperatures and a diel water temperature change with R adjusted by the van't Hoff-Arrhenius equation. The difference between 8°C and 20°C is a reduced range of O_2 saturation and $\delta^{18}O$-O_2 values over the diel cycle at the colder temperature. This is solely a result of the difference in solubility of O_2 at different temperatures, which in turn affects G. Although P and R are held constant in this example, the dissolved O_2 pool is 30% larger at 8°C than at 20°C, thus observed changes in $\delta^{18}O$-O_2 values are smaller. This is a pool dilution effect whereby the same amount of O_2 is produced by P and consumed by R but as a portion of the total O_2 pool a smaller fraction is metabolically cycled. As a result of the increased solubility of O_2, a comparatively smaller fraction of the total O_2 is derived from the photosynthetic input of O_2 with very low $\delta^{18}O$-O_2 values and thus the daytime portion of the concentration curve deviated less from the nighttime portion of the curve. At night, the same R produces a smaller decline in O_2 saturation because of the increased solubility at lower temperatures. The total amount of G (aerial rates of influx and efflux) remains the same because differences in the dissolved O_2 concentration and saturation are balanced by the same k. The slope of the nighttime curve is the same at 8°C and 20°C.

The effect of a typical sinusoidal diel temperature change from 8°C (night) to 20°C (2.5 h after solar noon) is to increase the diel change in O_2 saturation and decreased the diel change in $\delta^{18}O$-O_2 relative to the constant temperature regimes. There is only a small effect on the mean O_2 saturation and $\delta^{18}O$-O_2 values but the shape is changed, including (1) an increased temporal offset of the maximum O_2 saturation and $\delta^{18}O$-O_2 minimum from solar noon, demonstrating that this offset is not only a function of k; (2) an earlier minimum O_2 saturation; (3) a decrease in the duration of a night-time O_2 saturation plateau; and (4) in a cross-plot of O_2 saturation vs. $\delta^{18}O$-O_2, a reduction in the overall slope of the curve but a greater difference between the daytime and nighttime portions of the curve. Although temperature is not an independent variable, it is important to take diel temperature changes into account because temperature is required to convert measurements of O_2 concentration into saturation. Shallow water bodies, such as ponds and rivers, may exhibit significant diel temperature changes (Venkiteswaran et al. 2007).

Net effects of the key environmental and biological parameters

The overall effect of the key parameters described above on diel O_2 saturation and $\delta^{18}O$-O_2 curves are not always intuitive, nor are the multiple combinations of these parameters, which are encountered in nature, easily grasped. Table 1 contains a generalized framework for assessing field diel O_2 and $\delta^{18}O$-O_2 curves without modeling. P, R, and G affect the diel magnitude of both O_2 saturation and $\delta^{18}O$-O_2 (the range of values and thus the length of curves). Dissolved O_2 isotopic fractionation factors (α_R and α_G) affect only the $\delta^{18}O$-O_2 of diels and because they are multiplied by R and k, respectively, are only as important as R and k are large. The $\delta^{18}O$-H_2O is similarly expressed relative to P and controls the comparative slope of the diel curve. Temperature controls O_2 solubility, affects R, and thereby modifies both the shape and location of the diel O_2 saturation and $\delta^{18}O$-O_2 curves in temporal and cross-plot figures. Venkiteswaran et al. (2007) provide details

[4] ⟨http://www.waterisotopes.org/⟩

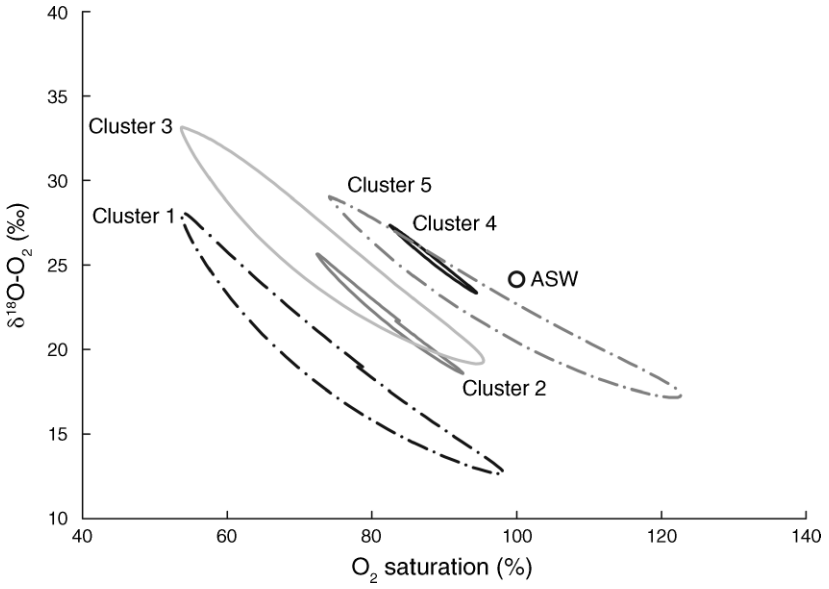

FIG. 8. Based on a synoptic study of New Zealand streams, Wilcock et al. (1998) organized the ecosystem health of their streams into five clusters based on complete linkage cluster analysis of their *P*, *R*, and *k* values (Table 2). Using average *P*, *R*, and *k* for these clusters, PoRGy was employed to generate diel O_2 saturation and $\delta^{18}O$-O_2 curves for each cluster. In order to make the curves more easily comparable, water temperature was set to 20°C, $\delta^{18}O$-H_2O value was −7‰, and α_R was set to 0.982 for all clusters, the same as the solid curve from Fig. 1. Air-saturated water (ASW) is shown as a black circle.

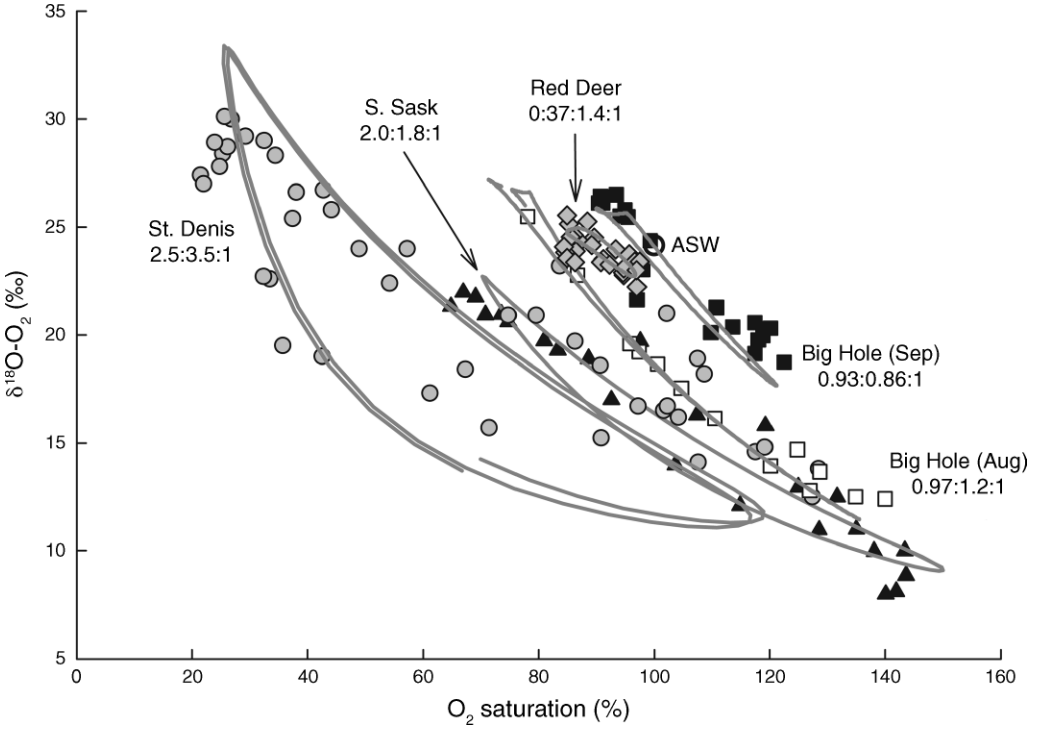

FIG. 9. Cross-plots of diel O_2 saturation and $\delta^{18}O$-O_2 and *P*:*R*:*G* ratios in three North American rivers and one prairie wetland: South Saskatchewan River 50 km downstream from Saskatoon, Saskatchewan, Canada, in July (black triangles; Venkiteswaran et al. 2007); Red Deer River at Bindloss, Alberta in August (gray diamonds; J. J. Venkiteswaran [*unpublished data*]); Big Hole River near Dickie Bridge, Montana in August (white squares) and September (black squares) (Parker et al. 2005); and wetland 50 at the St. Denis National Wildlife Area in September (gray circles; Venkiteswaran et al. 2007). The curves are best-fit solutions calculated with PoRGy. See Table 3 for more details. Air-saturated water (ASW) is shown as a black circle.

TABLE 3. Model input parameters and results for field examples shown in Fig. 9.

Input variables and results	South Saskatchewan River, 50 km downstream from Saskatoon, Saskatchewan, Canada (Venkiteswaran et al. 2007)	Big Hole River, Dickie Bridge, Montana, USA (Parker et al. 2005)	
Independently known input variables			
$\delta^{18}O\text{-}H_2O$ (‰)	−7	−17.0	−16.1
North latitude	52°30′37″	45°51′51″	45°51′51″
West longitude	106°24′53″	113°5′10″	113°5′10″
Day of year	197	268	234
Year	2004	2004	2004
Input variables adjusted to improve fit			
P_{max} ($mg \cdot m^{-2} \cdot h^{-1}$)	1640	1135	2585
R_{20} ($mg \cdot m^{-2} \cdot h^{-1}$)	340	255	885
k (m/h)	0.1072	0.2470	0.3479
α_R	0.998	0.975	0.987
Calculations from model fit			
P:R:G	1.97:1.78:1	0.93:0.86:1	0.97:1.2:1
P:R	1.11:1	1.08:1	0.79:1
P ($mg \cdot m^{-2} \cdot h^{-1}$)	425	180	584
R ($mg \cdot m^{-2} \cdot h^{-1}$)	382	166	740
G† ($mg \cdot m^{-2} \cdot h^{-1}$)	215	193	600
r^2‡	0.98 and 0.97	0.92 and 0.96	0.95 and 0.93

Note: P_{max} is the photosynthesis rate at theoretical maximum incident light, R_{20} is the nominal respiration rate at 20°C, and α_R is the dissolved O_2 community R isotopic fractionation factor.

† Gross G is the total influx and outflux, rather than the difference between influx and outflux.

‡ Values are for O_2 saturation and $\delta^{18}O\text{-}O_2$.

about how daily values of P, R, k, and α_R can be estimated from diel O_2 and $\delta^{18}O\text{-}O_2$ curves.

DISCUSSION

Point measurements are not useful in productive ecosystems

The metabolic balance of productive aquatic ecosystems is not likely to be adequately captured by daytime-only, random, or point measurements of O_2 saturation and $\delta^{18}O\text{-}O_2$ due to diel variations. Diel curves of O_2 concentration have been used previously to estimate metabolic balance (P:R) and P and R but have required various assumptions (e.g., assuming constant R and using empirical equations to estimate k). As a result, new methods and approaches to better constrain P and R, lessen the importance of the necessary assumptions, and identify ecosystems at risk from external stressors are required.

Diel $\delta^{18}O\text{-}O_2$ studies can also be useful in aquatic ecosystems that do not exhibit a diel change in every season. The lack of a diel change combined with $\delta^{18}O\text{-}O_2$ sets limits on the P, R, and k required to suppress diel changes in both O_2 and $\delta^{18}O\text{-}O_2$ (e.g., the Amazon River in Quay et al. [1995]). In such ecosystems, P must be low enough that the $\delta^{18}O\text{-}O_2$ value does not change significantly and either (1) R and G must be

TABLE 4. Summary of P, R, and k ranges for different ecosystems.

Ecosystem	P (mmol $O_2 \cdot m^{-2} \cdot d^{-1}$)	R (mmol $O_2 \cdot m^{-2} \cdot d^{-1}$)	G (as k_{600} [cm/h] or as $k_{2,20°C}$ [h^{-1}])	References
Lakes and ponds: planktonic	0–620	5–256	k_{600}: 0.5–11	P, R: Carignan et al. (2000), López-Archilla et al. (2004) P: Wetzel (2001), Welch (1968) R: Pace and Prairie (2005), Welch (1974) G: Cole and Caraco (1998), Matthews et al. (2003)
Creeks, streams, and rivers	0.3–2000	1–1353	k_{600}: 2–50 $k_{2,20°C}$: 0.0083–300	P, R: Allan (1996) P: Wetzel (2001), Davis (2002) P, G: Wilcock et al. (1999) P, R, G: Mulholland et al. (2001) G: Wilcock et al. (1995), Melching and Flores (1999)

Notes: Most metabolic rates were determined directly by measurements of O_2 instead of carbon and subsequent conversion to O_2. The k values were determined directly via tracer experiments or high-frequency measurements of wind speed combined with mass balance and site-specific equations for converting wind speed; k_{600} is k (in units of distance per time) normalized to a Schmidt number of 600 (the Schmidt number of CO_2 at 20°C in freshwater) and is a common format of expressing k for lakes; $k_{2,20°C}$ is the k value (in units of per time) normalized to 20°C for O_2 (a Schmidt number of 530) and is a common format of expressing k for rivers.

TABLE 3. Extended.

Wetland 50, St. Denis National Wildlife Area, Saskatchewan, Canada (Venkiteswaran et al. 2007)	Red Deer River, Bindloss, Alberta, Canada
0	−17.1
51°13′	50°52′58″
106°16′1″	110°16′33″
271	230
2000	2003
830	210
200	154
0.0093	0.1569
0.985	0.989
2.5:3.5:1	0.37:1.4:1
0.73:1	0.27:1
105	46
143	170
41	125
0.96 and 0.93	0.97 and 0.40

approximately equal if O_2 is undersaturated or (2) G must be much greater than R if O_2 is fully saturated.

P:R:G is better than P:R

Differences in ecosystem sensitivity to stressors due to the inherent balance between P, R, and G can be easily visualized in a cross-plot. The framework summarized in Table 1 was applied to a set of stream clusters for illustration purposes. Wilcock et al. (1998) described five stream clusters based on 23 rural lowland streams in agriculturally developed catchments in order to categorize streams according to their ability to withstand dissolved O_2 stressors and still maintain minimum acceptable environmental dissolved O_2 concentrations, a measure of ecosystem health. To group streams according to the similarity of processes controlling stream dissolved O_2 concentrations, they performed complete linkage cluster analysis of P, R, and k: all determined by analysis of diel dissolved O_2 curves. Here, PoRGy was used to generate steady-state diel $\delta^{18}O$-O_2 curves for these stream clusters using their values of P, R, and k, information about stream morphometry, and water temperature. A $\delta^{18}O$-H_2O of −7‰, and an α_R of 0.982 were assumed for all clusters for comparability (Table 2; Fig. 8). The parameters yield either large (clusters 1, 3, and 5) or small (cluster 2 and 4) diel curves. However, the size of the diel curve is not only related to community structure and metabolic rates, but also to G and thus to sensitivity to external stressors.

The diel curves for each cluster are clearly distinct but represent five snapshots along a continuum of possible diel curves. There is some overlap in the cross-plot between the diel curves (clusters 2 and 3, and clusters 4 and 5) but the lengths of these curves differ greatly.

Two comparisons are made to illustrate that the clusters depend simultaneously on P, R, and G: clusters 1 and 3, and clusters 3 and 5. Clusters 1 and 3 have nearly identical ranges in O_2 saturation: below 60% at night and peaking close to 100% after solar noon. From an O_2 saturation standpoint these stream clusters are indistinguishable from each other. However, in a cross-plot these clusters are separated in $\delta^{18}O$-O_2 by 5‰. This indicates that cluster 1 has a greater P:G ratio and a greater P:R ratio than cluster 3. Thus k is likely much slower in cluster 1 than in cluster 3 and hence cluster 1 is more sensitive to external stressors that affect k than is cluster 3 even though they have identical nighttime minimum O_2 saturation values. Stressors that cause an increase in R, such as increased BOD load or nutrients causing an increase in P, would have a much greater impact on cluster 1 than cluster 3.

Clusters 3 and 5 have very different ranges of O_2 saturation: 60–95% and 75–125%, respectively. However their range of $\delta^{18}O$-O_2 values is similar: 20–33‰ and 18–30‰. In a cross-plot, these clusters are separated with cluster 5 being closer to ASW but the mechanism for this separation is not intuitive. Community metabolism rates and k must be higher in cluster 5 than in cluster 3 because the diel curve of cluster 5 has a similar size while being closer to ASW than cluster 3. Stressors that could cause decreases in the nighttime O_2 minimum would have a much greater impact on cluster 3 than cluster 5 because of its slower k. Also, stressors that could reduce k in cluster 5 pose a risk to the nighttime O_2 minimum because of high R.

Diel curves can overlap for reasons other than just P and R (e.g., different k, significant temperature change, or a combination of variables). Field data from other regions can be compared to the Wilcock et al. (1998) clusters in order to generalize about the role of P:R:G in aquatic ecosystems. Field data collected from several North American aquatic ecosystems are presented in Fig. 9 and Table 3 along with best-fit solutions from PoRGy: the South Saskatchewan River 50 km downstream from Saskatoon, Saskatchewan (Venkiteswaran et al. 2007); the Big Hole River near Dickie Bridge, Montana (Parker et al. 2005); wetland 50 at the St. Denis National Wildlife Area, Saskatchewan (Venkiteswaran et al. 2007; see Plate 1); and the Red Deer River near Bindloss, Alberta (J. J. Venkiteswaran, *unpublished data*). These data clearly reveal that different types of aquatic ecosystems (in P:R:G terms) fall on different locations on an O_2 saturation vs. $\delta^{18}O$-O_2 cross-plot.

The inclusion of $\delta^{18}O$-O_2 in these diel studies makes visually interpreting the diel data easier than O_2 saturation alone, can allow for identifying important effects such as disturbances by following an ecosystem temporally or spatially, presents the clusters and ecosystems as a continuum described by P:R:G, and visually relates the ecosystems to each other and to some of the environmental influences that would cause them to change with time.

PLATE 1. Wetland 50 at the St. Denis National Wildlife Area, Saskatchewan, Canada in September 2000. Photo credit: Matthijs Vlarr and L. I. Wassenaar.

Ultimately, the determinant of O_2 dynamics in aquatic systems is the *P*:*R*:*G* ratio and not the conventional *P*:*R* ratio because of the inescapable connection between the water and the atmosphere in all aquatic ecosystems. Thus, one major advantage of including $\delta^{18}O$-O_2 data in diel sampling regimes is the ability to determine the *P*:*R*:*G* ratio with far greater precision than by O_2 saturation alone. Also, since *P*, *R*, and *G* differ between types of aquatic ecosystems (Table 4), various ecosystems plot differently in a cross-plot of O_2 saturation vs. $\delta^{18}O$-O_2. The stream clusters presented above clearly demonstrate that differences between ecosystems (including differences that are not apparent from O_2 saturation curves alone) can become apparent using $\delta^{18}O$-O_2 assays.

Measurements of $\delta^{18}O$-O_2 also provide a second and independent method of constraining *P, R*, and *k*. While *P*, *R*, and *P*:*R* can be estimated from O_2 saturation alone using conventional methods, the ratios and rates require *k* to be determined independently or be calculated from empirical models (e.g., Jha et al. 2004), numerical solutions (e.g., McBride and Chapra 2005), or nighttime regression (e.g., Odum 1956). This makes O_2 curve comparison between different ecosystems (or the same ecosystem across seasons) very difficult because *k* is needed to calculate *P* and *R* but the sensitivity to *k* is buried inside the assumptions and calculations. The use of *P*:*R*:*G* ratios explicitly recognizes that dissolved O_2 concentration also depends on *G* and that metabolism is better compared against an independent but ecosystem-relevant variable, *k*. Determining *P*:*R*:*G* with O_2 saturation and $\delta^{18}O$-O_2 data adds a second set of mass balance constraints when determining the rates of *P*, *R*, and *G*. Hence the addition of $\delta^{18}O$-O_2 provides a better-constrained estimate of aquatic metabolism and reaeration.

Many processes and factors including *P*, *R*, *P*:*R*, *k*, temperature, and light simultaneously affect diel curves. For example, both *k* and temperature will shift the maximum O_2 saturation from solar noon and both *R* and *k* will change the level and duration of a nighttime O_2 saturation plateau. Thus both the shape and mean of the diel temporal curves give information on what parameters are important. A confounding issue is that aquatic ecosystems are rarely at daily steady-state (i.e., they do not return to the same point every night) because they are meteorologically dependent (e.g., warming trend, flow-rate changes, cooling trend, cloudy periods). Thus, single diel O_2 studies are best done by including $\delta^{18}O$-O_2 and by switching to a transient model so that steady-state assumptions can be removed.

Conclusions

Six key environmental and biological parameters (*P*, *R*, *k*, α_R, $\delta^{18}O$-H_2O, and temperature) affect the shape, size, and location of diel O_2 saturation and $\delta^{18}O$-O_2 curves in complex and interactive ways. Understanding the effect of these key parameters on O_2 saturation and $\delta^{18}O$-O_2 elucidates important controls on aquatic ecosystems, allows for comparison between aquatic ecosystems, and aids the use of models (e.g., PoRGy) to determine quantitative estimates of ecosystem metabolic rates using real data. This framework is useful because different combinations of parameters can result in apparently overlapping diel curves. Thus both O_2 saturation and $\delta^{18}O$-O_2 are needed to disentangle potentially confounding influences.

The sensitivity of aquatic ecosystems to stressors was described in terms of the inherent balance between *P*, *R*, and *G* using five stream clusters described by Wilcock et al. (1998). Diel $\delta^{18}O$-O_2 curves can be used to identify aquatic ecosystems that may be more vulnerable to external stressors, such as ecosystems where *G* is small relative to *P* and *R* because (1) estimates of *k* are better constrained with a second mass balance and (2) *P*:*R*:G can be inferred from the size, shape, and location of a diel curve in a cross-plot. The general framework of the key parameters governing the diel O_2 saturation and $\delta^{18}O$-O_2 curves is an important tool for studies of aquatic ecosystem health.

ACKNOWLEDGMENTS

This work was funded by a National Science and Engineering Research Council of Canada Strategic Project Grant (S. L. Schiff and L. I. Wassenaar), Environment Canada (L. I. Wassenaar), and an Ontario Graduate Scholarship (J. J. Venkiteswaran). R. J. Wilcock kindly provided additional stream morphometry information.

Literature Cited

Allan, J. D. 1996. Stream ecology. First edition. Chapman and Hall, London, UK.

Andrews, S. S., S. Caron, and O. C. Zafiriou. 2000. Photochemical oxygen consumption in marine waters: a major sink for colored dissolved organic matter? Limnology and Oceanography 45:267–277.

Barton, B. A., and B. R. Taylor. 1996. Oxygen requirements of fishes in northern Alberta rivers with a general review of the adverse effects of low dissolved oxygen. Water Quality Research Journal of Canada 31:361–409.

Bennoun, P. 2002. The present model for chlororespiration. Photosynthesis Research 73:273–277.

Benson, B. B., D. Krause, Jr., and M. A. Peterson. 1979. The solubility and isotopic fractionation of gases in dilute aquatic solution. I. Oxygen. Journal of Solution Chemistry 8:655–690.

Bowen, G. J., L. I. Wassenaar, and K. A. Hobson. 2005. Global application of stable hydrogen and oxygen isotopes to wildlife forensics. Oecologia 143:337–348.

Brandes, J. A., and A. H. Devol. 1997. Isotopic fractionation of oxygen and nitrogen in coastal marine sediments. Geochimica et Cosmochimica Acta 61:1793–1801.

Carignan, R., D. Planas, and C. Vis. 2000. Planktonic production and respiration in oligotrophic Shield lakes. Limnology and Oceanography 45:189–199.

Carpenter, S. R., N. F. Caraco, D. L. Correll, R. W. Howarth, A. N. Sharpley, and V. H. Smith. 1998. Nonpoint pollution of surface waters with phosphorus and nitrogen. Ecological Applications 8:559–568.

Chapman, G. 1986. Ambient water quality criteria for dissolved oxygen. U.S. EPA 440/5-86-003, Washington, D.C., USA.

Chapra, S. C., and D. M. Di Toro. 1991. Delta method for estimating primary production, respiration, and reaeration in streams. Journal of Environmental Engineering ASCE 117: 640–655.

Chomicki, K. M., and S. L. Schiff. 2008. Stable oxygen isotopic fractionation during dissolved organic carbon photodegradation in stream waters. Science of the Total Environment, *in press*.

Churchill, M. A., H. L. Elmore, and R. A. Buchingham. 1962. The prediction of stream reaeration rates. Journal of Sanitation Engineering ASCE 88(SA4):1–46.

Clark, I., and P. Fritz. 1997. Environmental isotopes in hydrology. CRC Press, Boca Raton, Florida, USA.

Cole, J. J., and N. F. Caraco. 1998. Atmospheric exchange of carbon dioxide in a low-wind oligotrophic lake measured by the addition of SF_6. Limnology and Oceanography 43:647–656.

Davis, J. F. 2002. Factors affecting photosynthetic rates of periphyton in shallow steams of southeastern Pennsylvania. Water Environment Research 74:370–376.

del Giorgio, P. A., and R. H. Peters. 1994. Patterns in planktonic *P*:*R* ratios in lakes: influence of lake trophy and dissolved organic carbon. Limnology and Oceanography 39: 772–787.

Dodds, W. K. K., and E. B. Welch. 2000. Establishing nutrient criteria in streams. Journal of the North American Benthological Society 19:186–196.

Falkowski, P. G., and J. A. Raven. 1997. Aquatic photosynthesis. Blackwell Science, Malden, UK.

Guy, R. D., J. A. Berry, M. L. Fogel, and T. C. Hoering. 1989. Differential fractionation of oxygen isotopes by cyanide-resistant and cyanide-sensitive respiration in plants. Planta 177:483–491.

Guy, R. D., M. L. Fogel, and J. A. Berry. 1993. Photosynthetic fractionation of the stable isotopes of oxygen and carbon. Plant Physiology 101:37–47.

Hendricks, M. B., M. L. Bender, B. A. Barnett, P. Strutton, and F. P. Chavez. 2005. Triple isotope composition of dissolved O_2 in the equatorial Pacific: a tracer of mixing, production, and respiration. Journal of Geophysical Research 110: C12021.

Hendry, M. J., L. I. Wassenaar, and T. K. Birkham. 2002. Microbial respiration and diffusive transport of O_2, $^{16}O_2$, and $^{18}O^{16}O$ in unsaturated soils: a mesocosm experiment. Geochimica et Cosmochimica Acta 66:3367–3374.

Jha, R., C. S. P. Ojha, and K. K. S. Bhatia. 2004. A supplementary approach for estimating reaeration rate coefficients. Hydrological Processes 18:65–79.

Kendall, C., and T. B. Coplen. 2001. Distribution of oxygen-18 and deuterium in river waters across the United States. Hydrological Processes 15:1363–1393.

Kiddon, J., M. L. Bender, J. Orchardo, D. A. Caron, J. C. Goldman, and M. Dennett. 1993. Isotopic fractionation of oxygen by respiring marine organisms. Global Biogeochemical Cycles 7:679–694.

Knox, M., P. D. Quay, and D. Wilbur. 1992. Kinetic isotopic fractionation during air–water gas transfer of O_2, N_2, CH_4, and H_2. Journal of Geophysical Research 97:20335–20343.

Kroopnick, P., and H. Craig. 1972. Atmospheric oxygen: isotopic composition and solubility fractionation. Science 175:54–55.

Lane, G. A., and M. Dole. 1956. Fractionation of oxygen isotopes during respiration. Science 123:574–576.

Laws, E. A., M. R. Landry, R. T. Barber, L. Campbell, M. L. Dickson, and J. Marra. 2000. Carbon cycling in primary production bottle incubations: inferences from grazing experiments and photosynthetic studies using ^{14}C and ^{18}O in the Arabian Sea. Deep-Sea Research Part II 47:1339–1352.

López-Archilla, A. I., S. Mollá, M. C. Coleto, M. C. Guerrero, and C. Montes. 2004. Ecosystem metabolism in a Mediterranean shallow lake (Laguna de Santa Olalla, Doñana Nation Park, SW Spain). Wetlands 24:848–858.

Luz, B., and E. Barkan. 2000. Productivity with the triple-isotope composition of dissolved oxygen. Science 288:2028–2031.

Matthews, C. J. D., V. L. St.Louis, and R. H. Hesslein. 2003. Comparison of three techniques used to measure diffusive gas flux from sheltered aquatic surfaces. Environmental Science and Technology 37:772–780.

McBride, G. B., and S. C. Chapra. 2005. Rapid calculation of oxygen in streams: approximate delta method. Journal of Environmental Engineering ASCE 131:336–342.

Melching, C. S., and H. E. Flores. 1999. Reaeration equations derived from U.S. Geological Survey database. Journal of Environmental Engineering ASCE 125:407–414.

Miles, C. J., and P. L. Brezonik. 1981. Oxygen consumption in humic-colored waters by a photochemical ferrous-ferric catalytic cycle. Environmental Science and Technology 15: 1089–1095.

Morse, N., W. B. Bowden, A. Hackman, C. Pruden, E. Steiner, and E. Berger. 2007. Using sound pressure to estimate reaeration in streams. Journal of the North American Benthological Society 26:28–37.

Mulholland, P. J., et al. 2001. Inter-biome comparison of factors controlling stream metabolism. Freshwater Biology 46:1502–1517.

O'Connor, D. J., and W. Dobbins. 1958. Mechanism of reaeration in natural streams. American Society of Civil Engineering Transactions 123:641–684.

Odum, H. T. 1956. Primary production in flowing waters. Limnology and Oceanography 1:102–117.

Pace, M. L., and Y. T. Prairie. 2005. Respiration in lakes. Pages 103–121 *in* P. A. del Giorgio and P. J. le B. Williams, editors. Respiration in aquatic ecosystems. Oxford University Press, Oxford, UK.

Parker, S. R., S. R. Poulson, C. H. Gammons, and M. D. Degrandpre. 2005. Biogeochemical controls on diel cycling of stable isotopes of dissolved O_2 and dissolved inorganic

carbon in the Big Hole River, Montana. Environmental Science and Technology 39:7134–7140.

Quay, P. D., S. Emerson, D. O. Wilbur, C. Stump, and M. Knox. 1993. The $\delta^{18}O$ of dissolved O_2 in the surface waters of the subarctic Pacific: a tracer of biological productivity. Journal of Geophysical Research 98:8447–8454.

Quay, P. D., D. O. Wilbur, J. E. Richey, and A. H. Devol. 1995. The ^{18}O:^{16}O of dissolved oxygen in rivers and the lakes in the Amazon Basin: determining the ratio of respiration to photosynthesis rates in freshwater. Limnology and Oceanography 40:718–729.

Rizzo, W. M., S. K. Dailey, G. J. Lackey, R. R. Christian, B. E. Berry, and R. L. Wetzel. 1996. A metabolism-based trophic index for comparing the ecological values of shallow-water sediment habitats. Estuaries 19:247–256.

Sarma, V. V. S. S., O. Abe, A. Hinuma, and T. Saino. 2006. Short-term variation of triple oxygen and gross oxygen production in the Sagami Bay, central Japan. Limnology and Oceanography 51:1432–1442.

Stevens, C. L. R., D. Schultz, C. Vanbaalen, and P. L. Parker. 1975. Oxygen isotope fractionation during photosynthesis in a blue-green and a green alga. Plant Physiology 56:126–129.

Tobias, C. R., J. K. Böhlke, and J. W. Harvey. 2007. The oxygen-18 isotope approach for measuring aquatic metabolism in high-productivity waters. Limnology and Oceanography 52:1439–1453.

Venkiteswaran, J. J., L. I. Wassenaar, and S. L. Schiff. 2007. Dynamics of dissolved oxygen isotopic ratios: a transient model to quantify primary production, community respiration, and air–water exchange in aquatic ecosystems. Oecologia 53:385–398.

Wanninkhof, R. 1992. Relationship between wind speed and gas exchange over the ocean. Journal of Geophysical Research 97:7373–7382.

Welch, E. B., and J. M. Jacoby. 2004. Pollutant effects in freshwater: applied limnology. Third edition. Spon Press, London, UK.

Welch, H. E. 1968. Use of modified diurnal curves for the measurement of metabolism in standing water. Limnology and Oceanography 13:679–687.

Welch, H. E. 1974. Metabolic rates of arctic lakes. Limnology and Oceanography 19:65–73.

Wetzel, R. G. 2001. Limnology: lake and river ecosystems. Third edition. Academic Press, San Diego, California, USA.

Wilcock, R. J., G. B. McBride, J. W. Nagels, and G. L. Northcott. 1995. Water quality in a polluted lowland stream with chronically depressed dissolved oxygen: causes and effects. New Zealand Journal of Marine and Freshwater Research 29:277–288.

Wilcock, R. J., J. W. Nagels, G. B. McBride, K. J. Collier, B. T. Wilson, and B. A. Huser. 1998. Characterisation of lowland streams using a single-station diurnal curve analysis model with continuous monitoring data for dissolved oxygen and temperature. New Zealand Journal of Marine and Freshwater Research 32:67–79.

Wilcock, R. J., J. W. Nagels, H. J. E. Rodda, M. B. O'Connor, B. S. Thorrold, and J. W. Barnett. 1999. Water quality of a lowland stream in a New Zealand dairy farming catchment. New Zealand Journal of Marine and Freshwater Research 33:683–696.